UNDERSTANDING THE LINK BETWEEN PROCESS PARAMETERS, MICROSTRUCTURE AND MECHANICAL PROPERTIES OF LASER SINTERED PA12 PARTS THROUGH X-RAY COMPUTED TOMOGRAPHY

MICHELE PAVAN[1, 2], TOM CRAEGHS[1], PETER VAN PUYVELDE[3], JEAN-PIERRE KRUTH[2], WIM DEWULF[2]

[1]Materialise NV; Technologielaan 15, 3001 – Leuven, Belgium ; E-mail: michele.pavan@materialise.be, tom.craeghs@materialise.be
[2] Department of Mechanical Engineering, KU Leuven; Celestijnenlaan 300, 3001 - Leuven, Belgium; E-mail: jean-pierre.kruth@kuleuven.be , wim.dewulf@kuleuven.be
[3] Department of Chemical Engineering, KU Leuven; Celestijnenlaan 200, 3001-Leuven, Belgium; E-mail: peter.vanpuyvelde@cit.kuleuven.be

ABSTRACT: Laser Sintering is an Additive Manufacturing technique increasingly used to produce functional parts, with polyamide-12 (PA12) being by far the most processed material. It is common practice in industry to process a mix of recycled and virgin PA12 powder; however it is not yet fully understood how the Laser Sintering process parameters influence the microstructural composition for this mixture, namely the degree of crystallinity, the porosity characteristics and the distribution of the pores within the sintered parts. In this work X-ray Computed Tomography (CT) is used to investigate the porosity of tensile bars printed flatwise using a 50/50 mix of used and virgin PA12 processed with different Laser Sintering energy densities (EDs). Analysis of the pores characteristics and image processing of the CT-slices parallel to the building platform provide insights into the link between Laser Sintering process parameters, pores formation and their arrangement into the sintered polymer for different energy density levels. This information combined with the crystallinity values measured by Differential Scanning Calorimetry, gives a complete picture of the microstructure of the sintered material and its link with the resulting tensile properties.

KEYWORDS: X-ray Computed Tomography, Laser Sintering, Porosity Analysis, Non-Destructive Testing, PA12 , Differential Scanning Calorimetry

INTRODUCTION

Since its invention in the late eighties of last century, Laser Sintering (LS) has progressively moved from prototyping to the production of end use functional parts. The palette of processable materials is still limited compared with traditional manufacturing technologies like injection molding, with PA12 being by far the most processed material with a market share around 90%. LS process results are affected by a number of parameters that determine a spread in the quality of the parts produced. Goodridge et al. (2012) showed that the uneven distribution of pre-heating temperature on the powder bed platform can be correlated with lower tensile properties. In general variations of mechanical properties of the sintered semi-crystalline products can be due to both a different amount of polymer crystalline phase and different porosity levels as shown by Griessbach et al. (2010). Zarringhalam et al. (2006) showed how different LS process parameters can lead to a different degree of particle melt, resulting in residual crystals situated in the unmolten cores of the original powder particles. The presence of unmolten regions can be detected through Differential Scanning Calorimetry (DSC), because of their higher melting temperature compared with the newly formed crystals, which is mainly attributable to the different size and order of the crystallites. Gogolewski et al. (1980) showed how long annealing times at a temperature close to the melting temperature lead to an increase of the heat of melting and of the melting temperature in PA12 parts. Wegner et al. (2014) showed the temperature distribution in the printing volume to be not constant, leading to a variety of thermal histories for parts positioned at different positions within the build volume, which could potentially lead to a crystallinity variations in the sintered parts.

The choice of LS process parameters is also determining the level of porosity and relative density of the sintered parts. Dupin et al. (2012) showed how porosity and crystallinity of two different laser sintered PA12 powders change when the process parameters are changed, highlighting the strong influence of the particle size distribution and particle morphology on the porosity measured by CT, which showed a difference in average pore volume (μm^3) of one order of magnitude between the two virgin powders. Literature also reports on other cases where X-ray CT has been used to perform qualitative and quantitative porosity measurements on laser sintered PA12 parts. Ruesenberg et al. (2011) showed a difference in the porosity distribution between the core and the skin in a PA12 cube sintered using virgin PA2200 powder. Rouholamin et at. (2015) correlated the porosity levels and pore morphology measured using X-ray CT with the process parameters used to produce the parts using virgin PA2200 powder, finding a maximum pore dimension around 50 μm for all Energy

Proc. of the 2nd Intl. Conf. on Progress in Additive Manufacturing
Edited by Chee Kai Chua, Wai Yee Yeong, Ming Jen Tan, Erjia Liu and Shu Beng Tor

Published by Research Publishing, Singapore
ISSN: 2424-8967

Densities (EDs) investigated. It is clear that the combination of different PA12 powders and process parameters results in a range of possible microstructures with different porosity levels, pores size and morphology, and degree of crystallinity, hence leading to a variation of the mechanical response of the sintered parts. However, the available literature mainly focuses on virgin powders, while in industry it is common practice to process mix of recycled and virgin powders, due to the high price of the material. Verbelen et al. (2016) showed how some recycled PA12 powders present worse rheological properties (higher viscosities compared with virgin powders), which reduces the capabilities of the powder to produce dense parts, as reported by Kruth et al. (2007).
Until now, it remains difficult to make a link between the process parameters, the internal porosity and the resulting mechanical properties for PA12 powder mixtures traditionally used in industry. This work therefore presents an approach combining CT-based porosity measurements, DSC measurements and mechanical testing of tensile bars produced with a wide range of ED levels. The analysis of porosity statistics and image processing of CT slices allows to obtain a complete description of the influence of the LS process parameters on the porosity levels and distribution within the part, giving insights about pores formation and their arrangement in the sintered polymer. Information about crystallinity obtained through DSC analysis of the sintered parts moreover allows to have a complete picture of the microstructure composition, hence allowing to understand the link with the tensile properties of PA12 parts produced from a 50/50 mix between virgin and used powders.

MATERIALS AND METHODS

Production of the samples

Seven layers of four tensile bars each are produced using seven different ED levels on a P395 machine from EOS GmbH using a PA2200 PA12 powder with a mixing ratio of 50/50 between virgin and recycled powder, a layer thickness of 120 μm and a layer-alternated x and y scanning pattern. In order to minimize the effect of the temperature gradient within the building envelope and of the relative different thermal history on the crystallinity, the tensile bars have been printed flatwise at the center of the build platform. For the same reason the ordering of the layers doesn't follow the progressive increase in ED, but is instead chosen randomly, keeping the tensile bars produced with the same ED in the same layer. The process parameters used to produce the samples are summarized in Table 1.

ID sample	Height (Layer) (1-Top, 7-Bottom)	Hatching Laser Power (W)	Hatching Scanning Speed (mm/s)	Hatching Scan Spacing (mm)	Energy Density (mJ/mm^2)
ED20	1	18.0	3000	0.3	20
ED25	7	22.5	3000	0.3	25
ED30	6	27.0	3000	0.3	30
ED35	2	31.5	3000	0.3	35
ED40	3	36.0	3000	0.3	40
ED45	4	40.5	3000	0.3	45
ED50	5	45.0	3000	0.3	50

Table 1 Laser Sintering process parameters used to produce the tensile bars.

X-ray Computed Tomography

CT scans have been taken using a 225 keV CT machine from Nikon Metrology using a Molybdenum target, a voltage of 70 kV, a current of 200 μA and 1500 projections. The magnification of x20 yields a voxel size of 10 μm. The reconstruction of the projections into the 3D voxel volume is performed using CT Pro 3D software from Nikon Metrology. The datasets are analyzed using VGStudio max 2.2 from Volume Graphics GmbH, where the closed porosity is calculated using the defect detection module. Further analysis with Matlab code involves: pores volume distribution, pores sphericity distribution, pores distribution along the printing direction and cumulative porosity maps which have been created using the approach described by Dewulf et al. (2016).

Differential Scanning Calorimetry

The PA12 melting and crystallization behavior has been observed by DSC (Q2000 from TA Instruments) on samples of 7 ± 0.5 g taken from the center of each tensile bar (+10°C and -10°C temp. rate with 5 min. dwell at max. temp. of 220°C). The heat of melting in J/g, is converted into a percentage of crystallinity by dividing it by the heat of melting for a 100% crystalline specimen, which is equal to 209.3 J/g according to Gogolewski et al. (1980).

RESULTS AND DISCUSSION

Influence of process parameters on the degree of crystallinity

Figure 1 shows DSC melting peaks of central samples of the tensile bars for EDs ranging from 20 to 35 mJ/mm^2. For EDs below 35 mJ/mm^2 the presence of a second peak around 189°C is noticable, which decreases with increasing ED. This peak is referable to unmolten crystallites of the original powder as shown by Zarringhalam et al. (2006). For EDs equal to or higher than 35 mJ/mm^2 this second peak disappears, ensuring full melting of the original powder. Since the degree of crystallinity in the powder is much higher (ca. 47 %) than the common values for sintered parts (25-28) (Van Hooreweder et al. (2013)), one could expect the crystallinity to be maximum for the lowest ED and to decrease for higher EDs until reaching a stable value at EDs that allow the full melting of the original powder. However Figure 1 (right) does not support this hypothesis, especially for the tensile bars sintered at the lowest ED. This could be explained by the different thermal histories of the bars, which according to Gogolewski et al. (1980) strongly influences the melting temperature and the heat of melting. The production of parts by LS consists of two main phases: a printing phase, where the parts are actually printed, and a cooling phase, where the entire build has to cool down before removing the parts. These two phases determine different thermal histories of the parts according to their position within the build. The building envelope is heated by keeping its sides and bottom at a temperature around 150°C, which yields that zones built first undergo a longer thermal cycle than zones built last, with a difference which depends on the build height. Once the last layer is completed, the build has to cool down. Assuming a uniform insulation of the building envelope and taking into account the low thermal conductivity of the packed PA12 powder, the temperature at the sides of the envelope will decrease faster than at the center. The combination of these two phases determines a shorter thermal cycle with an average lower temperature for areas positioned at the top of the build compared to the other positions, which could be translated in a lower degree of crystallinity. The tensile bars produced at the lowest ED (20 mJ/mm^2) have been printed at the top of the build which might explain the deviation from the expected trend. The same considerations can be made for the tensile bars printed with an ED of 35 mJ/mm^2, which are posioned in the second layer from the top and present a lower crystallinity than expected.

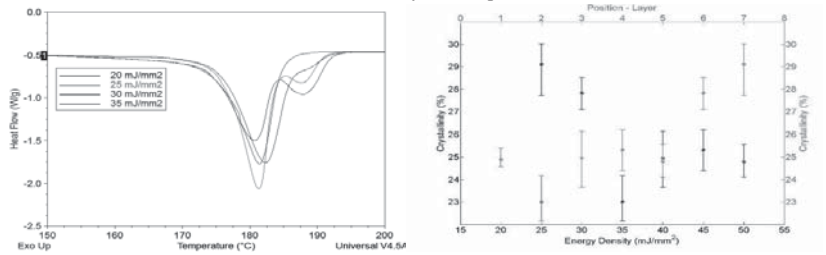

Figure 1 Melting peaks of central piece of the tensile bars produce different EDs (left). Degree of crystallinity of tensile bars depending on the ED used to produce them and their position within the build (right).

Influence of LS process parameters on porosity

Figure 2 (left) shows the presence of an optimal ED which minimizes the porosity content. Figure 2 (right) shows the porosity distribution along the thickness of the tensile bar (top to bottom), i.e. along the printing direction, for three of the EDs used. The porosity distributions are obtained by calculating the porosity of each CT-slice exported parallel to the powder bed platform (slicing direction equal to the printing direction). Due to the small voxel size (10µm) compared to the layer thickness (120µm) it is possible to assess the evolution of the porosity both along the thickness of the tensile bar and for each sintered layer thickness.

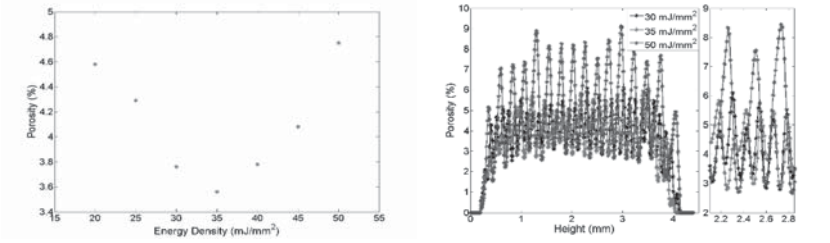

Figure 2 Porosity measured using VGStudio max software on CT datasets of central regions of interest of the tensile bars (left). Porosity distributions along the tensile bars thickness for EDs equal to 30 mJ/mm^2, 35 mJ/mm^2 and 50 mJ/mm^2 (right).

For EDs below 35 mJ/mm^2, the porosity distribution shows a regular pattern with a wavelength equal to the layer thickness. From an ED equal to 35 mJ/mm^2 onwards there is a progressive transition towards a pattern with a wavelenght equal to twice the layer thickness, which is complete for an ED equal to 50 mJ/mm^2. Figure 3 shows porosity maps of tensile bars produced with 30 mJ/mm^2 (left) and 50 mJ/mm^2 (right), taken perpendicular to the length of the bar. A porosity map is obtained by taking a number of parallel CT-cross-sections thru a part; the porosity information coming from each CT-slice are added together in order to calculate a cumulative porosity map, where each pixel represents the average porosity of the corresponding pixels of the entire stack of CT-slices analyzed. Figure 3 shows again a fluctuation of the porosity with a frequency corresponding to the layer thickness at 30 mJ/mm^2 and twice the layer thickness at 50 mJ/mm^2.

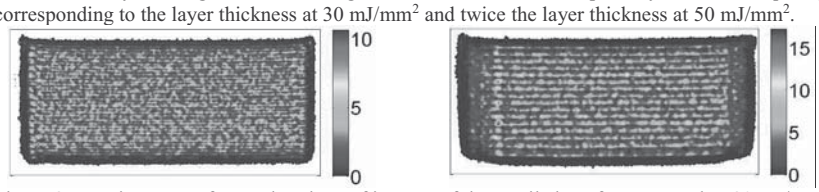

Figure 3 Porosity maps of central regions of interest of the tensile bars for ED equal to 30 mJ/mm^2 (left) and 50 mJ/mm^2 (right). Color-bar refers to the percentage of porosity.

Figure 4 (left) shows how the sphericity of the pores increases with the ED. Figure 4 (right) shows how the pores volume distribution progressively shifts towards larger pores sizes with increasing ED. This suggests that the creation of the pattern shown in Figure 2 (right) could be due to the progressive coalescence of pores of two subsequent layers leading to the formation of larger pores mainly located in between these layers. As shown in Figure 2 (left) this mechanism leads to an increase of the porosity in the microstructure. Ho et al. (1999) have shown a similar decrease in density while increasing the ED above 90 mJ/mm^2 suggesting as possible cause the polymer degradation. Vasquez et al. (2013) calculated the volumetric ED for degradation of PA2200 PA12 to be 0.43 J/mm^3; translating the maximum ED used in our test in volumetric ED by dividing it by the layer thickness we obtain 0.417 J/mm^3. However, since the CO_2 laser irradiates the powder bed from the top of the layer, there is the formation of a gradient between top and bottom of the layer, which can be up to several hundred degrees according to a simulation done by Williams et al. (1998) for bisphenol-A - polycarbonate processed at 80 mJ/mm^2. Even if this gradient disappears in fractions of a second (time depends on the parameters used), the energy delivered locally could lead to a degradation of the polymer and release of gas.

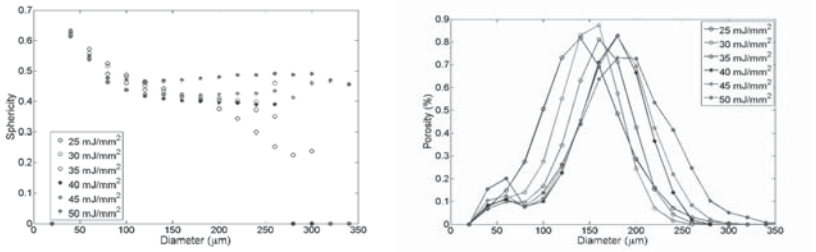

Figure 4 Pores sphericity distributions (left) and pores volume distributions (right) (assuming a spherical shape of the pores) of central region of interests of the tensile bars for different EDs.

Figure 4 (right) shows a higher porosity related to the small pores for an ED equal to 50 mJ/mm^2 compared to the other EDs, which could be due to the nucleation of small gas bubbles in the material due to the local thermal degradation of the polymer. If this is the case, this degradation could partially influence the measured porosity. However, the mechanism which involves the coalescence of pores of two subsequent layers starts already at 35 mJ/mm^2, which suggests the two phenomena are not related to each other. Anyway, further investigations are needed in order to understand why this mechanism keeps repeating every two layers generating the regular pattern shown.

Tensile properties

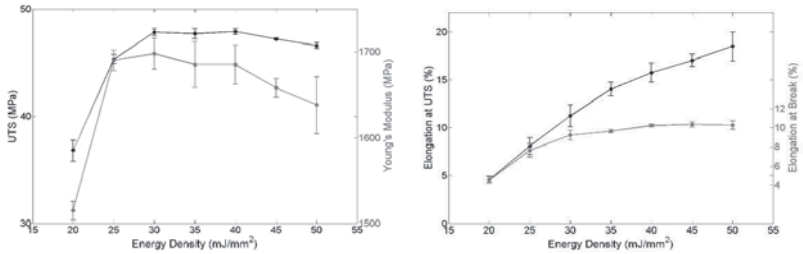

Figure 5 Mechanical properties of the tensile bars for different EDs.

Figure 5 shows low tensile properties for the lowest ED used in the test, which can probably be attributed to a very poor connection between the layers. Moreover a slight decrease of Young Modulus (E) and Ultimate Tensile Strength (UTS) is noticeable for high ED values, which can be attributed to the higher porosity and lower crystallinity of these specimens. It is known that for semi-crystalline thermoplastic polymers like PA12, an increase in the degree of crystallinity determines an increase in the strength and stiffness of the polymer (increase of UTS and E) as the secondary bonding is enhanced when the molecular chains are closely packed and organized into the lamellae of the spherulites. The increase in the degree of crystallinity leads also to a decrease of the ductility of the polymer. However, these considerations cannot explain the increase in elongation at break for EDs above 35 mJ/mm^2, since the porosity keeps increasing and the degree of crystallinity remains stable. Possible contributors to this ductility increase could be the improved inter-diffusion of the polymer chains at the interface between the layers and potential rearrangement of the pores in the microstructure.

CONCLUSIONS

The investigations allowed to describe the effect of the process parameters on both the crystallinity and the porosity present in the microstructure, as well as their link to the tensile properties. Differential scanning calorimetry measurements pointed out that for energy densities above 35 mJ/mm^2, there are no residual crystals from the original powder. Porosity measurements based on computed tomography showed 35 mJ/mm^2 to be the optimal energy density to minimize the porosity content. Further increasing the energy density yields a progressive change of the porosity distribution from a regular pattern every layer to another pattern reoccurring only every two layers, with the pores becoming progressively more spherical. Although the energy densities used are below the degradation energy density reported in literature, it is possible that locally this value could be exceeded. The higher porosity related to the small pores of the maximum ED used in the test could suggest an initial degradation of the polymer leading to the nucleation of small gas bubbles in the material. This phenomena could partially contribute to the increase of porosity for the maximum ED. Moreover the progressive shift of the pores volume distributions towards larger pore sizes, suggests that the change in the porosity distribution pattern is due to the coalescence of the voids of two subsequent layers. Further study will focus on understanding why this phenomena happens every second layer, as well as clarifying the reason of the improved ductility for high energy densities.

ACKNOWLEDGMENTS

This work was funded by the EU 7th Framework Programme FP7-People under ITN grant agreement No. 607817 (INTERAQCT).

REFERENCES

Dewulf, W., Pavan, M., Craeghs, T. & Kruth, J.-P., (2016), "Using X-ray Computed Tomography to improve the porosity level of polyamide-12 laser sintered parts", CIRP Annals Manufacturing Technology, [SUBMITTED].

Dupin, S., Lame, O., Barrès, C. & Charmeau, J.Y., (2012), "Microstructural origin of physical and mechanical properties of polyamide 12 processed by laser sintering", European Polymer Journal, 48(9), pp. 1611-1621.

Gogolewski, S., Czerniawska, K. & Gasiorek, M., (1980), "Effect of annealing on thermal properties and crystalline structure of polyamides. Nylon 12 (polylaurolactam)", Colloid & Polymer Science, 258, pp. 1130-1136.

Goodridge, R.D., Tuck, C.J. & Hague, R.J.M., (2012), "Laser sintering of polyamides and other polymers", Progress in Materials Science, 57(2), pp. 229-267.

Griessbach, S., Lach, R., & Grellmann, W., (2010), "Structure-property correlations of laser sintered nylon 12 for dynamic dyw testing of plastic parts", Polymer Testing, 29, pp. 1026-1030.

Ho, H.C.H., Gibson, I. & Cheung, W.L., (1999), "Effects of energy density on morphology and properties of selective laser sintered polycarbonate", Journal of Materials Processing Technology, 90, pp.204-210.

Kruth, J.P., Levy, G., Klocke, F. & Childs, T., (2007), "Consolidation phenomena in laser and powder-bed based layered manufacturing", CIRP Annals - Manufacturing Technology, 56(2), pp.730-759

Rouholamin, D. & Hopkinson, N., (2015), "An Investigation on the suitability of micro-computed tomography as a non-distructive technique to assess the morphology of laser sintered nylon parts", Journal of Engineering, p.665.

Ruesenberg, S., Schmidt, L. & Schmid, H.J., (2011), "Mechanical and Physical properties - A way to asses quality of Laser Sintered Parts", SFF 2011, pp. 239-251.

Van Hooreweder, B., Moens, D., Boonen, R., Kruth, J.-P., & Sas, P., (2013), "On the difference in material structure and fatigue properties of nylon specimens produced by injection molding and selective laser sintering", Polymer Testing, 32, pp. 972-981.

Vasquez, M., B, Haworth, B. & Hopkinson, N., (2013), "Methods for quantifying the stable sintering region in laser sintered polyamide-12", Polymer Engineering and Science, 53, pp. 1230-1240.

Verbelen, L., Dadbakhsh, S., Van den Eynde, M., Kruth, J.-P., Goderis, B. & Van Puyvelde, P., (2016), "Characterization of polyamide powders for determination of laser sintering processability", European Polymer Journal, 75, pp. 162-174.

Wegner, A., & Witt, G., (2014). "Understanding the decisive thermal processes in laser sintering of polyamide 12", 30th International Conference of the Polymer Processing Society. Cleveland

Williams, J.D. & Deckard, C. R., (1998), "Advances in modeling the effects of selected parameters on the SLS process", Rapid Prototyping Journal, 4, pp. 90-100

Zarringhalam, H., Hopkinson, N., Kamperman, N. F. & Vlieger, J.J., (2006), "Effects of processing on microstructure and properties of SLS Nylon 12", Materials Science and Engineering: A, 435-436, pp. 172-180